PHILOSOPHICAL TRANSACTIONS OF THE ROYAL SOCIETY A MATHEMATICAL, PHYSICAL & ENGINEERING SCIENCES

Spectroscopy and dynamics of the Rydberg states of C_2H_2 and their relevance to astrophysical photochemistry

Niloufar Shafizadeh, Jean-Hugues Fillion, Dolores Gauyacq and Stelios Couris

Phil. Trans. R. Soc. Lond. A 1997 **355**, 1637-1658
doi: 10.1098/rsta.1997.0081

Spectroscopy and dynamics of the Rydberg states of C_2H_2 and their relevance to astrophysical photochemistry

By Niloufar Shafizadeh[1], Jean-Hugues Fillion[1]†, Dolores Gauyacq[1] and Stelios Couris[2]

[1]*Laboratoire de Photophysique Moléculaire, Bât. 213, Université de Paris-Sud, 91405 Orsay Cedex, France*

[2]*Foundation for Research and Technology-Hellas, Institute of Electronic Structure and Laser, P.O. Box 1527, 71110 Heraklion, Crete, Greece*

In order to understand the role of the Rydberg states in the photodestruction of acetylene in circumstellar envelopes, we have investigated the spectroscopy of some of the *ungerade* and *gerade* states by resonant multiphoton ionization in a magnetic bottle photoelectron spectrometer. The *ungerade* ns + nd Rydberg supercomplexes of C_2H_2 have been investigated by one-colour (3 + 1) multiphoton ionization, in the energy region 79 500–87 000 cm^{-1}. Our spectral data show a very different behaviour of the various components of these supercomplexes towards predissociation. The highly excited *gerade* nf Rydberg states have been observed for the first time, by two-colour (3 + 1′) multiphoton ionization. A value for the adiabatic ionization potential, 91 956 cm^{-1}, has been obtained from the observed series limit and from earlier high-resolution infrared data on the ground state of the ion. This value is 4 cm^{-1} higher than the one measured by ZEKE spectroscopy. The apparent broadening of the observed Rydberg features may originate both from Zeeman 'broadening' of the non-penetrating nf complexes and from predissociation. The np Rydberg states, for which observation is fully allowed in the same spectral region, do not appear in the ionization signal at least in the low-n range, most probably because of their very short lifetime. In the high-energy region, spectral congestion, probably involving p–f mixing, occurs.

1. Introduction

The acetylene molecule is an important constituent of carbonated star envelopes, as has been shown by the infrared detection in IRC+10 216 (Ridgway *et al.* 1976). In this circumstellar medium, C_2H_2 and its photodissociation product C_2H are thought to be the main reservoir from which carbon-rich interstellar dust forms (Omont 1993). The photodestruction of C_2H_2 by the galactic UV radiation has been established as the dominant mechanism leading to the radical C_2H (Lafont *et al.* 1982; Huggins *et al.* 1984; Truong-Bach *et al.* 1987; Beiging & Nguyen-Q-Rieu 1988). Nevertheless, the

† Present address: Observatoire de Paris (DAMAp) et URA 812 du CNRS, 5 Place J. Janssen, 92195 Meudon Cedex, et Université de Cergy-Pontoise, France.

Phil. Trans. R. Soc. Lond. A (1997) **355**, 1637–1658
Printed in Great Britain

photodissociation mechanism in the first few absorption bands of acetylene is still, after a considerable number of laboratory investigations, only partially understood. A large number of measurements have been carried out using 193 nm photolysis light and concluded that the production of C_2H and H was the major channel among all dissociation processes at this excitation energy (Balko *et al.* 1991 and references therein). Other studies performed at different wavelengths (Okabe 1981, 1983) reported the observation of other competing relaxation channels leading to formation of the products $C_2 + H_2$, as well as to formation of excited triplet vinylidene radicals (Fahr & Laufer 1986). In the region of the Rydberg states, the decay mechanisms are even less well understood.

Photodissociation cross section measurements performed between 153 nm and 193 nm by using low-resolution synchrotron radiation revealed the role of resonant molecular structure, i.e. predissociation, especially at low temperature (Wu *et al.* 1989). Photoabsorption and fluorescence studies in the region 105–155 nm led to the same conclusion (Suto & Lee 1984). Thus, the Rydberg states which exhibit a strong absorption cross section in the VUV (Nakayama 1964) must play a major role in the circumstellar photodestruction of acetylene as gateway states towards dissociation. Indeed, one-colour resonant multiphoton ionization (REMPI) studies have pointed out that above 9.4 eV, the Rydberg states of acetylene undergo very fast predissociative decay (Orlando *et al.* 1987; Ashfold *et al.* 1987).

Rydberg states of acetylene converging to the $\tilde{X}^2\Pi_u$ state of $C_2H_2^+$, belong to the $D_{\infty h}$ group and, therefore, can be separated into two vibronic symmetry species, the *ungerade* and the *gerade* states, as shown in figure 1. The singlet *ungerade* states have been the subject of many investigations, both experimental (Wilkinson 1958; Dance & Walker 1973; Gedanken *et al.* 1973; Colin *et al.* 1977; Herman & Colin 1981, 1982) and theoretical (Kammer 1970; Demoulin & Jungen 1974; Demoulin 1975; Peric *et al.* 1984). In particular, many UV absorption bands involving the $ns\sigma_g$, $^1\Pi_u$ and $nd\delta_g$, $^1\Pi_u$ series for the four isotopomers C_2H_2, C_2D_2, $^{13}C_2H_2$ and C_2HD have been rotationally analysed, while other absorption bands involving the $nd\sigma_g$, $^1\Pi_u$ and $nd\pi_g$, $^1\Sigma_u^+$ series appear completely diffuse for all n values (Colin *et al.* 1977; Herman & Colin 1982). More recent REMPI studies involving one-colour three-photon excitation have been carried out on the *ungerade* Rydberg states (Ashfold *et al.* 1985, 1986; Orlando *et al.* 1986, 1987; Fillion *et al.* 1996), and allowed for the observation of new electronic components of the ns and nd series, namely the $nd\delta_g$, $^1\Phi_u$ state (Ashfold *et al.* 1985) and the $nd\pi_g$, $^1\Delta_u$ state (Fillion *et al.* 1996).

The lowest *gerade* np Rydberg states of acetylene have been observed by two-photon REMPI, either by using one-colour excitation (see Ashfold *et al.* 1987), or, by using two-colour excitation, through the intermediate $\tilde{A}\,^1A_u$ state (Takahashi *et al.* 1992). For this class of states, REMPI experiments have revealed an efficient decay channel above 9.4 eV, precluding the observation of any ionization signal from Rydberg states above $n = 4$ (actually, only one component of the 4p complex could be observed by Ashfold *et al.* (1987)). It has to be noted that this experimental search by REMPI has been limited to the energy region below 90 000 cm^{-1}, i.e. to Rydberg states with $n \leqslant 7$. In figure 1, the energy diagram of all observed singlet Rydberg states converging to the first ionization limit emphazizes the lack of information about the *gerade* Rydberg states.

Spectral data on the two lowest *ungerade* 4s + 3d and 5s + 4d supercomplexes, observed by one-colour (3 + 1) REMPI at a better resolution than the earliest work of Orlando *et al.* (1987), will first be discussed. Then, observation of new *gerade*

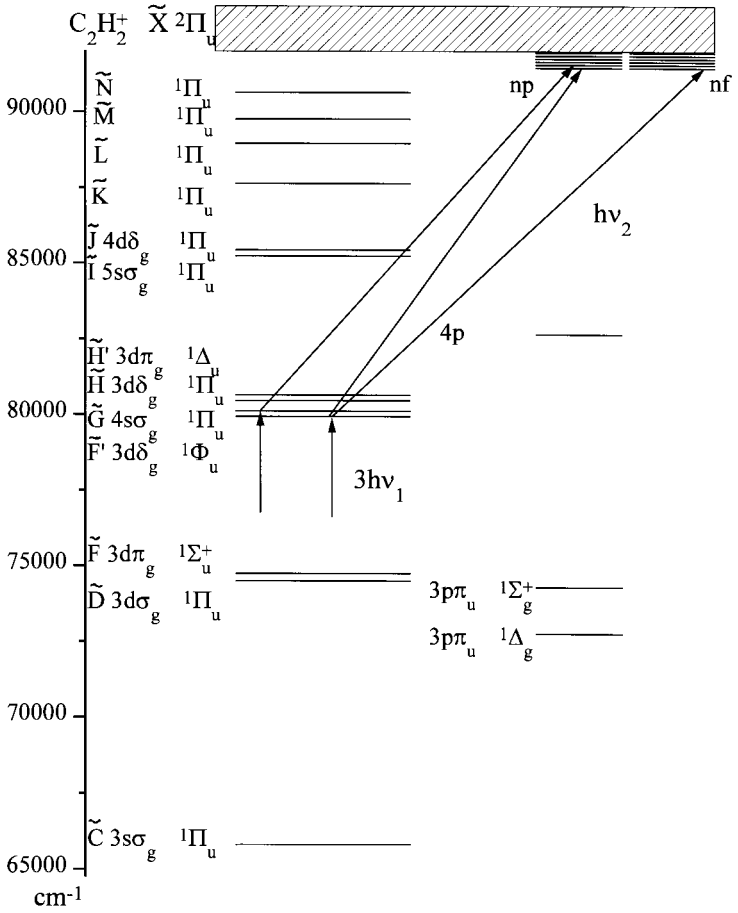

Figure 1. Energy diagram of the observed singlet Rydberg states of acetylene between 65 000 and 91 950 cm^{-1}. The high-lying *n*p and *n*f *gerade* states, unobserved up to now, are discussed in the text.

Rydberg series below the ionization limit will be presented together with a preliminary analysis. The data presented in this paper show very different lifetimes for the various Rydberg states.

2. Experiment

Both one- and two-colour experiments were performed in a 'magnetic bottle' electron spectrometer, which has been described elsewhere (Guizard *et al.* 1991). Acetylene, C_2H_2, diluted in acetone (liquid air), flowed through a 2 mm orifice into the vacuum chamber at room temperature. Typical operating pressure in the ionization chamber was about 6×10^{-4} mbar for the one-colour experiment and 10 times higher for the two-colour experiment. No attempt to purify C_2H_2 was made in this experiment.

The laser system consisted of two excimer (LUMONICS PM 886) pumped dye lasers (Lambda Physik, FL2002, for the three-photon excitation and Quantel TDLII for the probe beam in the two-colour experiment) operated at 15 Hz. Three-photon pumping was performed in the 385–360 nm spectral region (QUI and DMQ dye

solutions) with a 4–8 mJ *maximum* average pulse energy and a laser bandwidth of $0.3\,\mathrm{cm}^{-1}$. After attenuating down to *ca.* 150 μJ per pulse (for the strongest origin bands), the laser was focused into the ionization chamber with a 15 cm focal length lens (uncoated Suprasil). The probe laser was operated in the near infrared, between 800 and 900 nm (LDS 821 dye solution). The probe beam, of average pulse energy between 380 and 470 μJ, was focused into the high-field region of the magnetic bottle with a 5 cm focal length lens (uncoated Suprasil), so that the focal volume of the probe beam was spatially overlapped by the focal volume of the pump beam. The energy variation of either dye laser with wavelength was controlled by means of a micro-joulemeter (Laser Precision Corporation RjP 700). No attempt was made to correct spectral intensities against laser output energy, but special care was taken to maintain a smooth and almost constant laser energy variation over each spectral scan.

The magnetic bottle spectrometer was mainly used as a 'zero-background' detector, as follows: the overall electron current was collected through a fast preamplifier (LECROY VV100BTB) and then time analysed. In the one-colour experiment, only the photoelectron signal arising from the $(3 + 1)$ ionization process in acetylene was detected as a function of the laser wavelength. The signal arising from impurities, especially acetone, and corresponding to a longer time-of-flight was outside the time gate for detection. In the two-colour experiment, two signals were observed at different photoelectron energies, corresponding to one- and two-colour ionization processes, respectively (as will be shown in § 3 *b* below). In this case, only the photoelectron signal arising from the two-colour ionization process (slow electrons) was recorded as a function of the probe laser wavelength. The signal of interest was digitized via an appropriate time gate and accumulated over several laser shots (around 60) in a CAMAC detection system interfaced with a microcomputer.

Absolute wavelength calibration was achieved by monitoring simultaneously the neon optogalvanic signal from a Fe–Ne hollow cathode.

3. Results and discussion

(*a*) *The ungerade* $(4s + 3d)$ *and* $(5s + 4d)$ *supercomplexes*

Figure 2 displays the $(3 + 1)$ photon REMPI spectrum of the $(4s + 3d)$ and $(5s + 4d)$ supercomplexes in the region 80 000–88 000 cm^{-1}. Origin bands and vibrational bands involving one or two quanta of the ν_2 and ν_1 modes, i.e. the C–C and C–H symmetric modes, respectively, are observed in this figure. This spectrum, recorded at higher resolution than the cooled acetylene spectrum obtained earlier by Orlando *et al.* (1987), shows a number of strong and weak bands. Our experimental conditions of low pressure, room temperature and low laser intensity, significantly improved the quality of the spectra on what concerns resolution and rotational structure. In particular, comparison between the observed band profiles and rotational band profile simulations allowed the characterization of upper state vibronic symmetry in the case of non-overlapped bands, as well as an estimate of the individual rotational linewidths. As an example, two bands are displayed at a larger dispersion, with their corresponding simulated spectra, in the inserts of figure 2.

The origin bands of the lowest supercomplex $(4s + 3d)$ have been analysed in a previous paper (Fillion *et al.* 1996). A new electronic component, the $3d\pi\ ^1\Delta_u$ state, was characterized on the basis of rotational analysis, polarization studies and spectral isotopic shift of the two isotopomer C_2H_2 and C_2D_2, origin transitions.

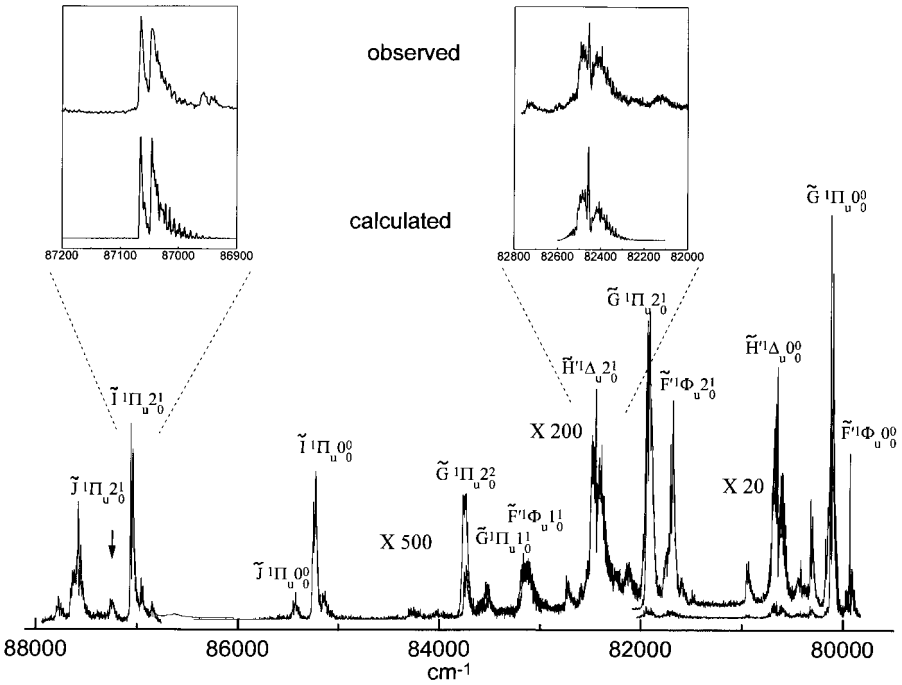

Figure 2. (3 + 1) photon ionization spectrum of acetylene in the energy region of the 4s + 3d and 5s + 4d supercomplexes. This spectrum is a composite of several laser scans corresponding to different dye solutions. Relative band intensities can be compared only within a single scan; approximate multipying factors are given to the different spectra with respect to the first one, which starts at 80 000 cm^{-1}. The spectra displayed at higher dispersion in the two inserts exhibit the rotational structure of the 2^1_0 bands for the upper $\tilde{I}\,^1\Pi_u$, 5sσ and $\tilde{H}'\,^1\Delta_u$, 3dπ states. The corresponding simulated spectra have been calculated with linewidths of 2.5 cm^{-1} and 5 cm^{-1}, respectively.

At the same time, Löffer *et al.* (1996) investigated the same supercomplex by using a sophisticated technique involving one-photon tunable narrow-band VUV laser excitation followed by hydrogen atom photofragment detection. Figure 3 shows the energy region of interest, investigated either by three-photon REMPI (figures 3*a–c*) or by one VUV photon, photofragment action spectroscopy (figure 3*d*). All intense features in this region correspond to electronic origin bands. In figure 3*a*, the three-photon spectrum, taken from Fillion *et al.* (1996), exhibits all electronic components of the (4s+3d) supercomplex except the transition to the 3dδ, $\tilde{H}\,^1\Pi_u$ state. Figure 3*b* shows the calculated spectrum based on the semi-united atom approximation. As pointed out by Fillion *et al.* (1996), this approximation gives an estimate of the relative transition intensities towards different electronic components belonging to the same 3d complex. In addition, the transition to the 4s, $\tilde{G}\,^1\Pi_u$ state is expected to have an electronic radial-transition moment similar to that of the transitions to the 3d components, if only the first rank tensors are considered (this statement is based on absorption data (see, for example, Colin *et al.* 1977)). We therefore assumed the same radial factor for the 4s and for the 3d states in our calculation of figure 3*b*. One can notice that the relative intensities of the 4s $^1\Pi_u$–$\tilde{X}\,^1\Sigma_g{}^+$ and the 3d $^1\Pi_u$–$\tilde{X}\,^1\Sigma_g{}^+$ transitions, shown in this figure, although very different from the (3 + 1) photon ionization spectrum of figure 3*a*, are in good agreement with the intensity

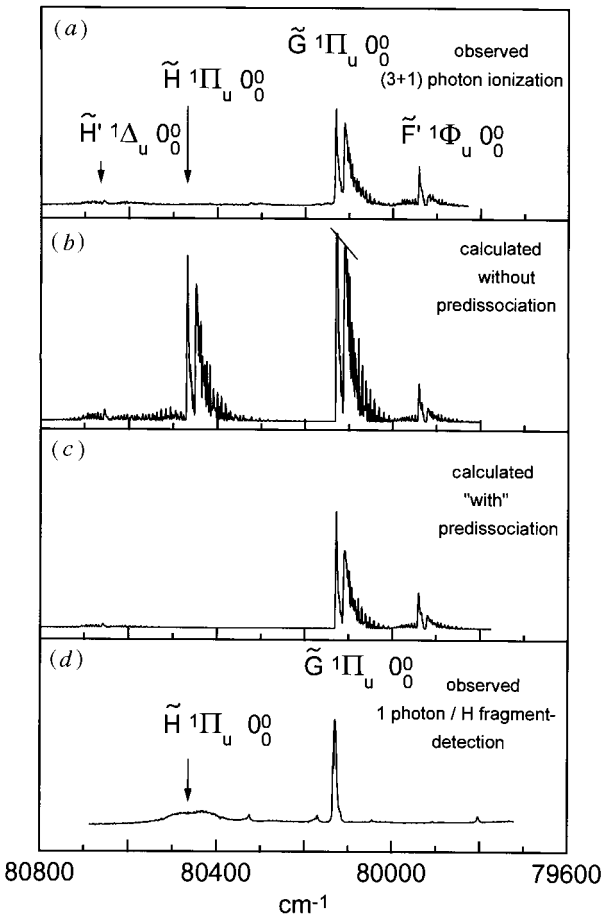

Figure 3. The upper members of the 4s + 3d supercomplex in the region 80 200 cm^{-1}: (*a*) observed (3 + 1) MPI spectrum; (*b*) calculated three-photon spectrum in the semi-united atom approximation (see text); (*c*) calculated (3+1) MPI spectrum for which predissociation has been taken into account as a loss factor in the ionization cross section, corresponding to $k_p/k_i = 0$ for the $\tilde{F}'\ ^1\Phi_u$ state, $k_p/k_i = 1.5$ for the $\tilde{G}\ ^1\Pi_u$ state, $k_p/k_i = 2$ for the $\tilde{H}'\ ^1D_u$ state and $k_p \gg k_i$ for the $\tilde{H}\ ^1\Pi_u$ state (k_p and k_i are the predissociation rate and ionization rate, respectively); (*d*) H-atom fragment action spectrum of the same supercomplex excited by tunable VUV light (spectrum adapted from Löffer *et al.* 1996).

ratio between the $(n + 1)$s and nd, $^1\Pi_u$–$\tilde{X}\ ^1\Sigma_g^+$, origin bands observed in absorption by Herman & Colin (1977).

Comparison between figures 3*a* and 3*b* indicates a significant decay channel for some of the Rydberg components, faster than the final photon's ionization channel. Indeed, in the absence of predissociation and third harmonic generation (this last possibility was ruled out by Fillion *et al.* (1996)), the three-photon $\tilde{H}\ ^1\Pi_u$–$\tilde{X}\ ^1\Sigma_g^+$ transition is expected to be very strong. On the other hand, even without invoking predissociation, the intensity of the $\tilde{H}\ ^1\Delta_u$–$\tilde{X}\ ^1\Sigma_g^+$ origin band is expected to be weak as compared with the nearby electronic components of the supercomplex, due to unfavourable angular factors in the three-photon transition moment. Figure 3*c* shows a calculated three-photon spectrum in which we have included the predissociation effect as a constant damping factor in the REMPI signal. In the case of the $\tilde{H}\ ^1\Delta_u$–

$\tilde{X}\,{}^1\Sigma_g^+$ transition, the predissociation lifetime of the $\tilde{H}\,{}^1\Delta_u$ upper state could be estimated to about 2–3 ps, both from the observed rotational linewidths and from our experimental conditions concerning the ionization step. For the $\tilde{G}\,{}^1\Pi_u$–$\tilde{X}\,{}^1\Sigma_g^+$ transition, the calculated intensities had to be lowered by a factor of 0.4, indicative of a small but still significant predissociation of the upper state (rotational linewidths were laser linewidth limited in this case). Finally, for the $\tilde{H}\,{}^1\Pi_u$–$\tilde{X}\,{}^1\Sigma_g^+$ transition, it was not possible to extract quantitative information about the upper state lifetime, because of the complete absence of this band in the REMPI experiment. In other words, it was not possible, by using our laser power conditions, to photoionize the $\tilde{H}\,{}^1\Pi_u$ state in a time scale short enough to compete with predissociation.

Information about the predissociation of this state could be obtained from the recent experiment of Löffer *et al.* (1996) where H fragment formation was detected after VUV excitation of the same supercomplex, as shown in figure 3*d*. Because of one-photon selection rules, only the ${}^1\Pi_u$ components of the supercomplex, which in turn undergo fragmentation, can be observed in this spectral region. Both transitions to the 4s, $\tilde{G}\,{}^1\Pi_u$ and the 3d, $\tilde{H}\,{}^1\Pi_u$ states were observed by H fragment action spectroscopy, with very different linewidths. The predissociation lifetime of the 3d, $\tilde{H}\,{}^1\Pi_u$ state has been estimated by Löffer *et al.* (1996) to be 52 fs while the lifetime of the 4s, $\tilde{G}\,{}^1\Pi_u$ state was expected to be longer than 2 ps. The observation of the $\tilde{G}\,{}^1\Pi_u$ state in the photofragment action spectrum confirms a significant predissociation of this state, albeit on a longer time scale than that of the $\tilde{H}\,{}^1\Pi_u$ state, as suggested from the above figures 3*b* and 3*c*. Nevertheless, the observed linewidths in our REMPI data show that the lifetime of the 4s, $\tilde{G}\,{}^1\Pi_u$ state is actually not much longer than 10–15 ps.

Löffer *et al.* (1996) measured a 1:1 ratio between the H-atom yield for the $\tilde{G}\,{}^1\Pi_u$ state and for the $\tilde{H}\,{}^1\Pi_u$ state, and pointed out that this was a surprising result, since these states have greatly different lifetimes. Actually, this result can be qualitatively understood as follows: Löffer *et al.* (1996) have ruled out multiphoton processes in their experiment, so that the above states can decay only by fluorescence or by other non-radiative decays, but not by photoionization. Since fluorescence takes place in a much longer time scale than a ps, both states primarily decay through predissociation into H fragments ($+C_2H$ or $+C_2, \ldots$), before any other relaxation mechanism has taken place (and even if it takes longer for the $\tilde{G}\,{}^1\Pi_u$ state to predissociate than for the $\tilde{H}\,{}^1\Pi_u$ state). Therefore, these states must exhibit equal H-atom yields which reflects their very close absorption cross sections. The different lifetimes bring a second and independent piece of information: the two states predissociate through different mechanisms. Indeed, if it was a direct process involving only one repulsive state, one would expect a very similar interaction strength between the continuum state and the vibrationless $\tilde{G}$ and $\tilde{H}$ states. This would most probably yield similar predissociation rates, since these states are separated by only 400 cm^{-1} and have parallel energy potential surfaces. An indirect process via at least one predissociative excited valence state of bent equilibrium geommetry is more likely to occur in this 10 eV energy region, in order to explain the different lifetimes. Such a process should indeed critically depend on the topology of the interacting surfaces.

Both types of experiments shown in figure 3 have finally led to complementary information on the structure and stability of all singlet components of the (4s + 3d) supercomplex of acetylene (except for the 3dπ, ${}^1\Sigma_u^-$ component which remains a dark state even by three-photon excitation). Linewidths have also been measured in the three-photon spectrum of figure 2 for 0_0^0 and 2_0^1 bands belonging to the (4s + 3d) and

Table 1. *Lifetimes for the electronic components of the lowest ns + nd supercomplex of C_2H_2, estimated from observed linewidths*

	$\nu_2 = 0$		$\nu_2 = 1$	
electronic state	energy (cm^{-1})	lifetime	energy (cm^{-1})	lifetime
$3d\delta$, $^1\Phi_u$	79 933	> 10 ps[c]	81 695	≈ 1 ps[c]
$4s\sigma$, $^1\Pi_u$	80 111	—	81 925	≈ 3 ps
$3d\delta$, $^1\Pi_u$	80 458	50 fs[b]	82 260	60 fs[b]
$3d\pi$, $^1\Delta_u$	80 637	≈ 3 ps	82 445	≈ 1 ps
$4d\delta$, $^1\Phi_u$	85 140	—	—	—-
$5s\sigma$, $^1\Pi_u$	85228	> 10 ps[a]	87 048	≈ 2 ps[a]
$4d\delta$, $^1\Pi_u$	85 424	≈ 10 ps[a]	87 241	≈ 2 ps[a]
$4d\pi$, $^1\Delta_u$	—	< 100 fs	—	—

[a]Herman *et al.* (1982).
[b]Löffer *et al.* (1996).
[c]Ashfold *et al.* (1985).

(5s + 4d) supercomplexes. These linewidths have been determined by comparison with simulated rotational band contours as shown in the inserts of figure 2. Corresponding lifetimes are summarized in table 1. One can see large differences, not only between the components of the same supercomplex, but also between members of the same $\ell\lambda$, Λ series, as well as between different vibrational levels of the same Rydberg state. Fillion *et al.* (1996) (see figure 5 of their paper) and Löffer *et al.* (1996) pointed out that the corresponding vibronic bands in the C_2D_2 isotopomer also exhibit different intensities and linewidths. As stated above, these observations suggest predissociation via indirect processes involving excited valence states of bent equilibrium geometry.

(*b*) *The gerade nf series below the ionization limit*

Relaxation mechanisms seem to be even more efficient for the *gerade* Rydberg states of acetylene. The lowest few *gerade* Rydberg states observed either by one-colour two-photon MPI spectroscopy (Ashfold *et al.* 1987) or by two-colour two-photon spectroscopy via the A state (Takahashi *et al.* 1992) are the $3p\pi$, $^1\Sigma_g^+$ and $^1\Delta_g$ states. Broad spectral features were tentatively assigned to the $3p\sigma$, $^1\Pi_g$ state by Takahashi *et al.* (1992). Finally a weak and diffuse signal was observed for the 4p complex by Ashfold *et al.* (1987). These authors suggested a fast non-radiative decay channel at energies above 76 000 cm^{-1}, between $n = 4$ and $n = 7$.

In the region of the lowest 3p complexes, the predissociation mechanism is likely to originate from strong Rydberg-valence interaction, as suggested by the *ab initio* calculations of Lievin (1992). In this energy region, the predissociative '*trans*-bent' $\tilde{C}\,^1A_g$ valence state, which has been experimentally characterized by Lundberg *et al.* (1992), exhibits strong avoided crossings with the 3p Rydberg components, namely the $3p\sigma$, $^1\Pi_g$, the $3p\pi$, $^1\Delta_g$ and $3p\pi$, $^1\Sigma_g^+$ states, along a '*trans*-bent' coordinate, i.e. in the ^1A_g symmetry. Similar valence-Rydberg interactions are expected to occur with a number of doubly excited valence states of *trans*-bent or *cis*-bent geometry in the higher energy region and could be responsible for the fast decay of the *gerade*

Rydberg states. On the other hand, such an electronic interaction arises mainly in the inner region for the electronic coordinate, the so-called core region, and, therefore, should decrease as n increases, roughly as $1/n^3$ (or, more precisely, as $1/n^{*3}$).

This argument further motivated our search for high *gerade* Rydberg states. In the region just below the IP, some Rydberg states may have a lifetime long enough to be observable by ionization techniques. Figure 4 shows the excitation scheme which was used for such an investigation. The well-characterized intermediate states $\tilde{G}\,{}^1\Pi_u$ $(4s\sigma)$ and $\tilde{F}'\,{}^1\Phi_u$ $(3d\delta)$ were chosen in order to probe most efficiently the high-lying np and nf states. Rotationally resolved three-photon spectra of these intermediate states allowed us to select well defined intermediate rotation-parity levels. As shown in figure 4, the high Rydberg states can be ionized by several mechanisms: photoionization by a further pump or probe photon, rotational autoionization, or collision-induced ionization. Although several other non-ionizing decay channels exist, as will be mentioned later, only one predissociation channel, into $C_2H + H$, has been indicated in this diagram. This channel represents all the loss channels for Rydberg states observed in this REMPI experiment.

A typical photoelectron spectrum, shown in figure 5, gives an example of our experimental excitation and detection conditions. In this spectrum, the pump wavelength was fixed at the band head of the three-photon $\tilde{F}'\,{}^1\Phi_u$–$\tilde{X}\,{}^1\Sigma_g^+$ transition, while the IR photon wavelength was chosen just above threshold in order to barely ionize the molecule. The sharp peak appearing at a time-of-flight of about 800 ns corresponds to resonant one-colour four-photon ionization by the pump beam, yielding electrons with a kinetic energy of 1.84 eV. The peak at about 2500 ns corresponds to a two-colour signal and originates from slow electrons (with a kinetic energy lower than 100 meV). Selective detection of this slow electron signal was performed via a time gate in order to suppress the background due to one-colour MPI. This figure also illustrates how the relative intensities of the pump and probe lasers were critical in the sense that the double resonance signal appeared only when the intensity of the probe beam was higher than that of the pump beam. Focusing conditions in the magnetic bottle allowed us to maintain the pump laser power just above threshold for the three-photon excitation step, but low enough to avoid saturation of the ionization step by one pump photon. No PES signal, arising from $(3\nu_1 + \nu_2 + \nu_2)$ or $(3\nu_1 + \nu_2 + \nu_1)$ ionization (see figure 4 for notation), was observed in any of our scans, thus, photoionization by an additional photon could be ruled out in our experiments. The Rydberg states are then most probably ionized by collision-induced ionization (in an energy range of the order of kT below threshold) or by rotational autoionization.

Two double resonance spectra of the high-lying *gerade* Rydberg states are shown in figure 6. They correspond to two different pump lines, one at 374.29 nm that is on the band head of the $\tilde{G}\,{}^1\Pi_u$–$\tilde{X}\,{}^1\Sigma_g^+$ transition, the other one at 375.18 nm that is on the band head of the $\tilde{F}'\,{}^1\Phi_u$–$\tilde{X}\,{}^1\Sigma_g^+$ transition. The IR laser was scanned between 865 nm and 843 nm when the $\tilde{G}$ state was pumped, and between 851 nm and 830 nm when the $\tilde{F}'$ state was pumped. As shown by the energy scale of figure 6, relative to the ground state, $J'' = 0$ level, exactly the same energy region below the IP was investigated from the two intermediate electronic states, although the two IR laser scans were shifted from each other.

The spectral range which exhibits resonant structures is very narrow. On the low-energy side, the ionization signal is very weak. When the excitation energy increases, the ionization signal increases rapidly, but then, the resonant structure becomes

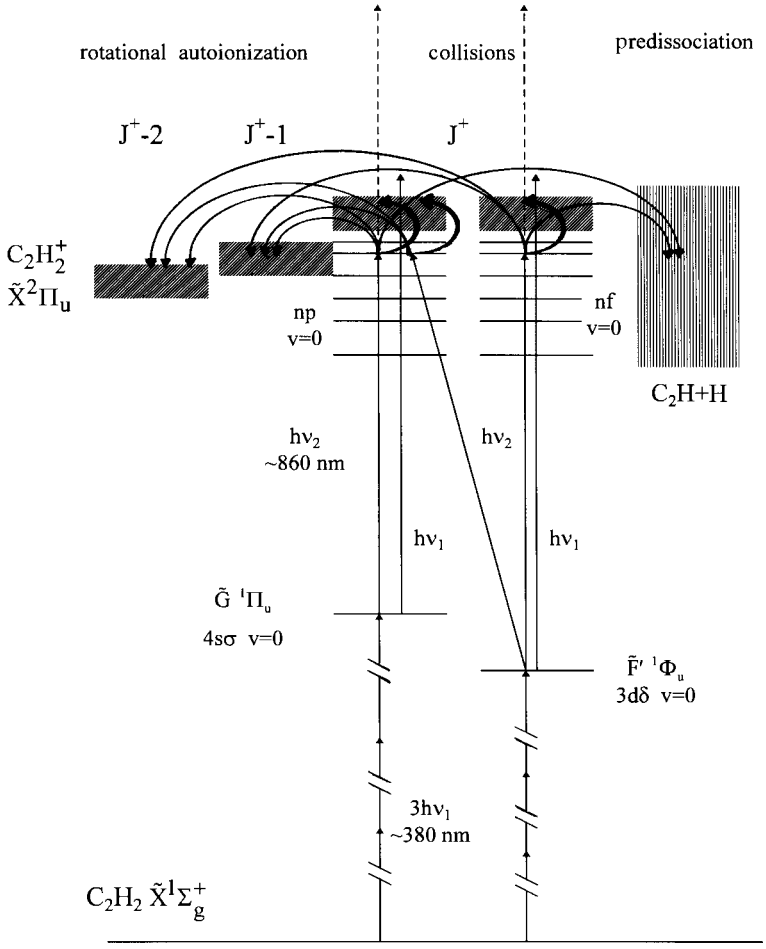

Figure 4. Excitation scheme for the high-lying *gerade* states of acetylene. The double resonance spectra of these Rydberg states were recorded via electron detection following collision-induced ionization or rotational autoionization (photoionization by a further blue or IR photon could be ruled out, see text). In this experiment, the dissociation channel is considered as a loss channel which competes with the ionization channel.

very crowded. This behaviour is rather typical of collision-induced ionization, which becomes increasingly efficient in a range of kT, i.e. around 200 cm^{-1} below the IP. Rotational autoionization can also contribute to the signal, since most of the observed resonant features are located above the adiabatic ionization threshold known from ZEKE measurements (Pratt *et al.* 1993). Pressure-dependent studies (Fillion 1995) show, however, that collisions are mainly responsible for the ionization of the Rydberg states in our experiment. Field ionization by stray E-fields can be ruled out for the observed Rydberg states ($20 \leqslant n \leqslant 45$), since it would correspond to an electric field of the order of 6 V cm^{-1}, which is too high a value for any residual field in our experiment. The external magnetic field does not ionize molecules, on the contrary it tends to increase the binding between the electron and the ion core (see, for example, Kleppner *et al.* 1983). Ionization by motional electric fields can also be ruled in the observed range of n.

The observed Rydberg series appear both regular and simple, which is very sur-

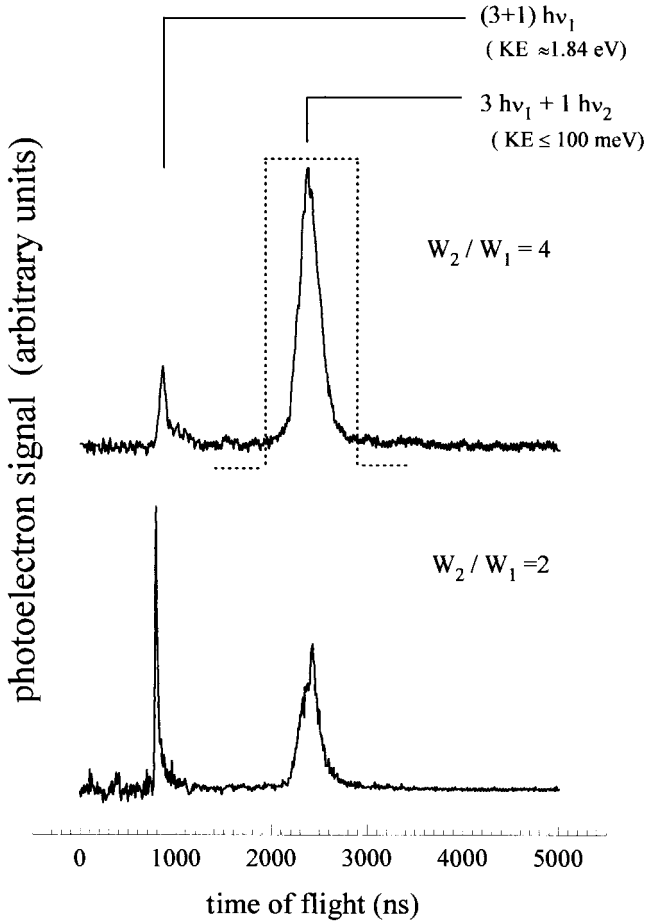

Figure 5. PES spectrum corresponding to the two-colour excitation scheme with $h\nu_1$ fixed at the band head of the three-photon $\tilde{F}\,{}^1\Phi_u$–$\tilde{X}\,{}^1\Sigma_g^+$ transition. The kinetic energy of both electron peaks and the ratio between the probe and pump laser beams are given for the two PES spectra. The dashed lines indicate the time gate used for the detection of the double-resonance signal.

prising if one considers that several intermediate rotational levels were pumped via the band heads and also on the basis of selection rules for Rydberg excitation, as will be discussed below. The second striking observation is that the two Rydberg spectra probed from two different electronic states with different symmetries are almost identical, at least in the 91 900–92 100 cm^{-1} excitation energy range. Concerning the expected (but not observed) complication due to the band head pump line, a simple explanation comes out from the *pure Rydberg character* of the two intermediate electronic states. The strongest rotational line within each electronic transition band head is $R(13)$, according to our rotational linestrength calculations (Fillion 1995). As indicated in figure 6, two other strong R lines are expected within each band head. The corresponding intermediate rotational levels are $J = 14$, 12 and 16 for the $\tilde{G}\,{}^1\Pi_u$ state and $J = 14$, 16 and 18 for the $\tilde{F}'\,{}^1\Phi_u$ state. As shown in table 2, the rotational spacings are very similar in the $\tilde{G}\,{}^1\Pi_u$ and $\tilde{F}'\,{}^1\Phi_u$ intermediate states, on one hand, and also very close to the corresponding rotational spacings of the $\tilde{X}\,{}^2\Pi_u$ ground state of the ion, measured by high-resolution infrared spectroscopy (Jagod *et al.* 1992), on the other hand. Therefore, all Rydberg series which are excited according to the same

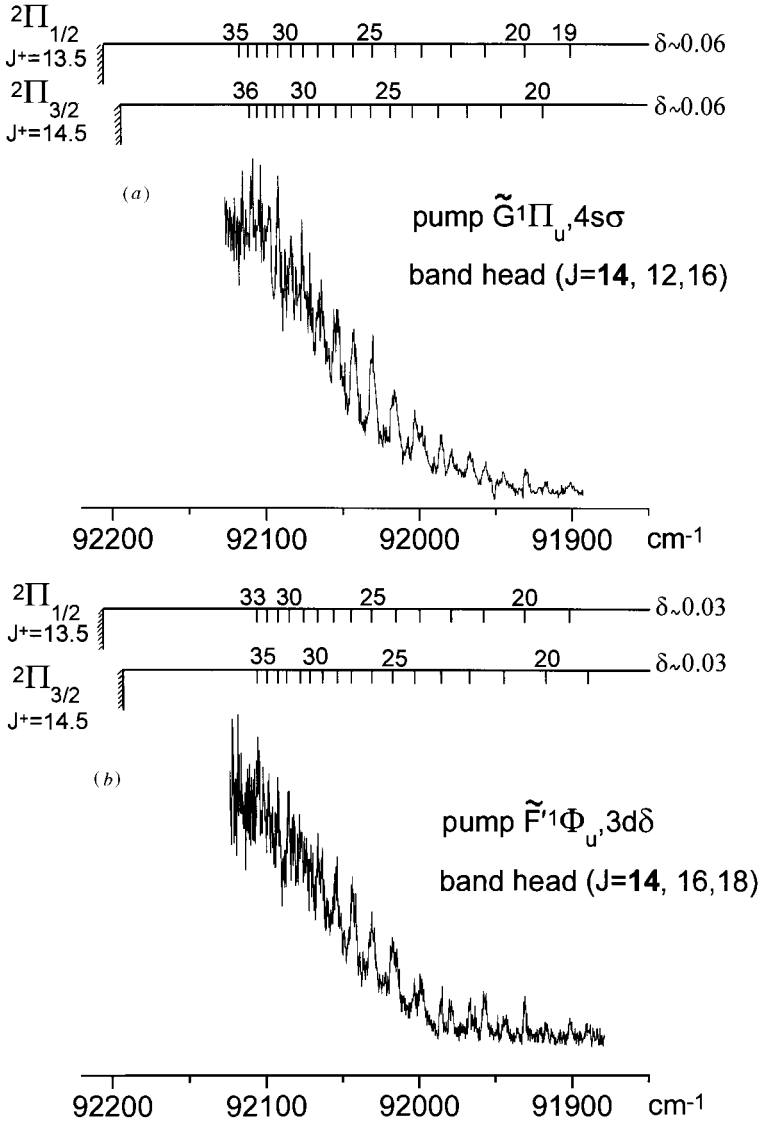

Figure 6. Two-colour MPI spectra of the Rydberg series of acetylene below IP: (*a*) pump line on the band head of the three-photon $\tilde{G}\,^1\Pi_u$–$\tilde{X}\,^1\Sigma_g^+$ transition; (*b*) pump line on the band head of the three-photon $\tilde{F}'\,^1\Phi_u$–$\tilde{X}\,^1\Sigma_g^+$ transition. Two identical prominent series converging towards the limits $^2\Pi_{1/2}$ ($J^+ = 13.5$) and $^2\Pi_{3/2}$ ($J^+ = 14.5$) with a near-zero quantum defect are observed from the two electronic intermediate states. The energy scale is given from $E = 0$ at the ground state, $J'' = 0$ level, and assuming that the rotational level $J = 14$ was pumped in the two intermediate states.

selection rule $J^+ - J$, from any of the J levels listed above, overlap almost exactly (within less than 1 cm^{-1}, i.e. less than the actual experimental linewidths).

The regular pattern observed in each spectrum is formed by two strong Rydberg series. After energy deperturbation from the Zeeman effect, which gives rise to a very small positive energy shift, as will be seen below, these series fit the Rydberg formula with an almost zero quantum defect and therefore can be assigned to non-penetrating nf series (the quantum defect for np series of acetylene being about 0.6). For this

Table 2. *Rotational energy spacings in the intermediate Rydberg states of C_2H_2 and in the ground state of the ion $C_2H_2^+$ (cm^{-1})*

J	$\Delta E_{\rm rot}(\tilde{G}\,^1\Pi_u)$	$\Delta E_{\rm rot}(\tilde{F}'\,^1\Phi_u)$	N^+	$\Delta E_{\rm rot}(\tilde{X}\,^2\Pi_{3/2})^a$ $J^+ = N^+ + \frac{1}{2}$	$\Delta E_{\rm rot}(\tilde{X}\,^2\Pi_{1/2})^a$ $J^+ = N^+ - \frac{1}{2}$
12			12		
	28.65	28.72		29.04	28.27
13			13		
	30.85	30.92		31.28	30.59
14			14		
	33.05	33.13		33.38	32.72
15			15		
	35.25	35.34		35.67	35.08
16			16		
	37.45	37.54		37.72	37.16
17			17		
	39.65	39.75		40.05	39.54
18			18		

[a]Jagod *et al.* (1991).

preliminary analysis, only one rotational intermediate level was considered in each Rydberg state $\tilde{G}\,^1\Pi_u$ and $\tilde{F}'\,^1\Phi_u$. This is the $J = 14$ level, which corresponds to the strongest pump line in both spectra. This assumption does not introduce any error since all Rydberg series probed from other J levels are shifted by the same energy difference as the intermediate J level and, therefore, are completely overlapped with the $J = 14$ series in the double resonance spectra. The Edlen plots shown in figure 7 for the two Rydberg series probed from the $\tilde{F}'\,^1\Phi_u$, $J = 14$ intermediate level, indicate an approximate quantum defect of 0.03 for these nf series. The two series limits, $^2\Pi_{3/2}$, $J^+ = 14.5$ and $^2\Pi_{1/2}$, $J^+ = 13.5$, are 92 194.0 cm^{-1} and 92 207.0 cm^{-1}, respectively, (the corresponding Edlen plots are marked by black squares in figure 7). These values seem to indicate that the adiabatic IP value measured from ZEKE experiments by Pratt *et al.* (1993) is too low by about 3.7 cm^{-1}. This is confirmed by the Edlen plots marked with open squares in figure 7, for which the rotational limit was calculated by adding the adiabatic IP value of 92 952 cm^{-1} (Pratt *et al.* 1993) to the accurate rotational spacings measured by IR spectroscopy of the ground state of the ion (Jagod *et al.* 1992). The analysis of other new nf series converging to different rotational limits (Fillion *et al.* 1997) yields the same conclusion, i.e. the spacings between the ionic rotational limits are in very good agreement with the IR analysis of the ionic ground state (Jagod *et al.* 1992), but the absolute energies are all shifted by +3.7 cm^{-1} from the term values calculated with the adiabatic IP measured from ZEKE experiment (Pratt *et al.* 1993). The new value for the lowest rotational level of the $\tilde{X}\,^2\Pi_{3/2}$ ion ground state, $J^+ = \frac{3}{2}$, determined from the above series limits and from the rotational analysis of Jagod *et al.* (1992), is 91 956($\pm$1) cm^{-1}.

The above analysis has been made by taking into account the Zeeman effect on the high Rydberg states due to the 0.93 T magnetic field in the ionization volume of the magnetic bottle. For a one-electron system, such as a Rydberg molecule, the

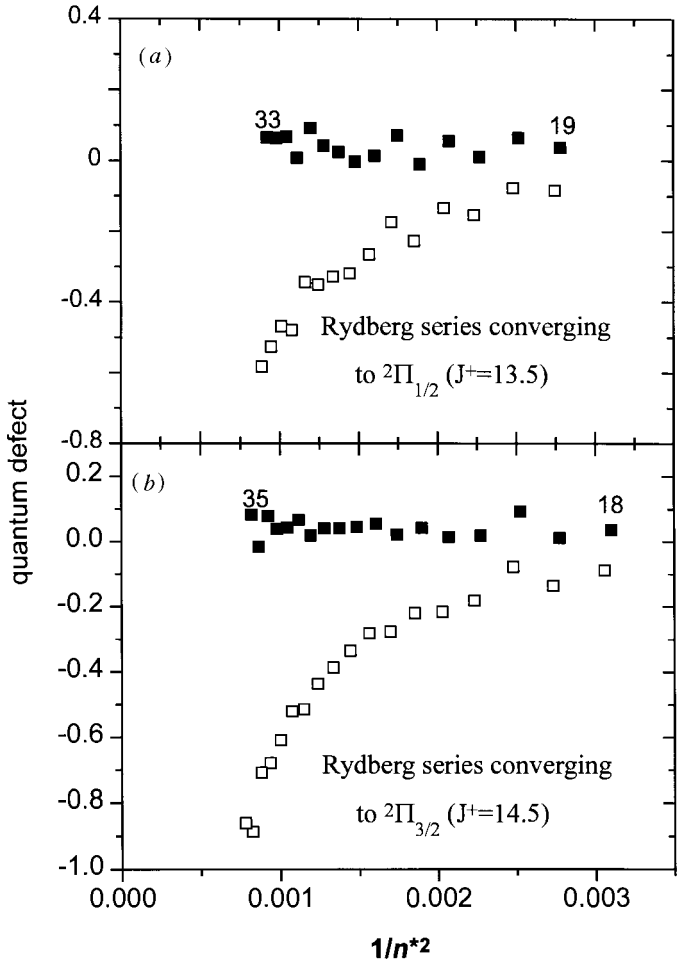

Figure 7. Edlen plot for the series probed from the $J = 14$ level of the intermediate $\tilde{F}'\,{}^1\Phi_u$ state. (*a*) series from $n = 19$ to 33 converging to the ion limit $^2\Pi_{1/2}$, $J^+ = 13.5$: ■, $T_\infty = 92\,207.0$ cm^{-1}; □, $T_\infty = 92\,203.1$ cm^{-1}. (*b*) series from $n = 18$ to 35 converging to the ion limit $^2\Pi_{3/2}$, $J^+ = 14.5$: ■, $T_\infty = 92\,194.0$ cm^{-1}; □, $T_\infty = 92\,189.4$ cm^{-1}. The two limits in (*a*) and (*b*) corresponding to the open square plots are calculated from Pratt *et al.* (1993) and Jagod *et al.* (1992) (see text). The abscissa corresponds to the dimensionless quantity $1/n^{*2} = (T_\infty - T_{\rm exp})/R$, where T_∞, $T_{\rm exp}$ and R are the ionization limit, the observed term values and the Rydberg constant, respectively.

Zeeman interaction consists of two terms

$$W_{\rm Zeeman} = \mu_{\rm B}(L_Z + 2S_Z)B + (e^2/8m)B^2r^2\sin^2\theta, \tag{3.1}$$

in which B is the magnetic field strength, $\mu_{\rm B}$ is the Bohr magneton, r and θ are the polar coordinate of the electron in the laboratory axis system, e and m are the charge and mass of the electron, and L_Z and S_Z are the projections of the electron orbital and spin angular momenta along the field axis.

The first term (linear Zeeman effect) is responsible for the splitting of the m_ℓ and m_s sublevels for an $n\ell$ Rydberg complex, at high-n values. The Zeeman splitting due to the electron spin, $\pm\mu_{\rm B}B$, is not observable in a Rydberg–Rydberg transition, since all Rydberg levels are equally shifted and transitions obey the selection rule

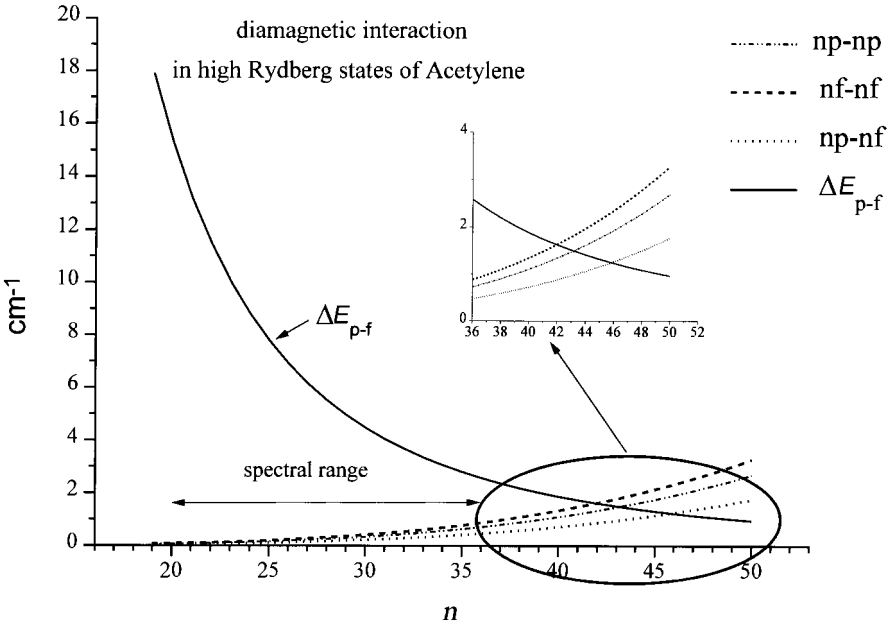

Figure 8. Quadratic Zeeman effect occurring in the 'magnetic bottle' for the high-np and nf Rydberg states: energy shift of the np and nf levels (diagonal matrix elements) and p–f mixing (off-diagonal matrix elements) versus n. The decreasing energy gap between np and nf levels as well as the observed spectral range are also shown.

$\Delta m_s = 0$. On the other hand, the m_ℓ structure arising from the linear Zeeman interaction can lead to a significant apparent broadening of the high-ℓ states at low resolution. For nf states of NO earlier probed in the same apparatus (Guizard *et al.* 1991), the m_ℓ Zeeman structure probed from 'd'-like orbitals extends over about $2\,\mathrm{cm}^{-1}$. Since the Rydberg transitions of figure 6 exhibit broad spectral features, we could not analyse in detail their linear Zeeman structure.

The second term, i.e. the so-called quadratic Zeeman effect or diamagnetic interaction, is negligible for such low Rydberg states as the intermediate 4s, $\tilde{G}\,{}^1\Pi_u$ and 3d, $\tilde{F}'\,{}^1\Phi_u$ states, but rapidly increases with n. It can therefore significantly affect the high-n Rydberg states. The diagonal matrix elements give rise to a positive energy shift of the $n\ell$ levels, while the off-diagonal matrix elements induce ℓ mixing with $\Delta\ell = \pm 2$. Within a 0.93 T magnetic field, the calculated Zeeman shift for np and nf states is given by

$$\left.\begin{aligned}\Delta E_{\mathrm{QZE}}(n\mathrm{p}) &= +4.30\times10^{-7}n^2(n^2-1)\\ \Delta E_{\mathrm{QZE}}(n\mathrm{f}) &= +5.25\times10^{-7}n^2(n^2-7)\end{aligned}\right\}\ (\mathrm{cm}^{-1}). \tag{3.2}$$

The quadratic Zeeman interaction between np and nf states also increases rapidly with n as

$$H_{\mathrm{QZE}}(n\mathrm{p}-n\mathrm{f}) = -2.81\times10^{-7}n^3\sqrt{n^2-1}\ (\mathrm{cm}^{-1}). \tag{3.3}$$

For $n = 20$, the np and nf states are shifted by $+0.07\,\mathrm{cm}^{-1}$ and $+0.08\,\mathrm{cm}^{-1}$, respectively, and for $n = 35$, the shift of the np and nf levels amounts to $+0.64\,\mathrm{cm}^{-1}$ and $+0.78\,\mathrm{cm}^{-1}$, respectively, as indicated in figure 8. The above correction has been taken into account in the analysis of the Rydberg series in order to determine the

correct zero-field ionization limit, with the assumption that we observed only nf Rydberg series, as suggested by the derived very small quantum defects.

The presence of the external magnetic field also affects Rydberg–Rydberg transition intensities through the selection rules. Indeed, without any external field, the upper Rydberg states are described by an intermediate coupling case between Hund's case (d) and Hund's case (e). Indeed, the value of the spin-orbit constant of the $^2\Pi_u$ ground state of the ion is $-30.7\,\mathrm{cm}^{-1}$, as measured by Cha *et al.* (1995). The spin-orbit splitting is of the same order of magnitude as the rotational spacing $2BJ^+$, for $J^+ = 14.5$, which means that the ion rotational structure moves from case (a) towards case (b) in the range of J values considered here. Although it is convenient to label the Rydberg series with the case (e) quantum numbers $\{\ell,\ J^+,\ \Omega^+\}$, the case (d) quantum number N^+ becomes meaningful for describing the $J = 14$ Rydberg series and Rydberg–Rydberg transition moments. The above descriptions are valid for a Rydberg electron strongly decoupled from the core so that it does not experience the core anisotropy. Thus, its angular momentum ℓ is quantized along the core rotation axis $\boldsymbol{N}^+$ rather than along the internuclear axis. When an external magnetic field is applied, the electron easily couples to the external field so that m_ℓ becomes a good quantum number. Guizard *et al.* (1991) have described previously the pure decoupled case (d) situation, and have derived the transition moment from pure case (b) to decoupled case (d) as:

$$\begin{aligned} D_{SM_S'\Lambda^{+\prime}\ell' m_{\ell'} N^{+\prime} M'_{N^+} \leftarrow SM_S\Lambda\ell N M_N} &= \mu(-1)^{N+N^{+\prime}-\Lambda-M_N+m_{\ell'}}\delta_{M_S'M_S}[(2\ell+1)(2\ell'+1)(2N+1)(2N^{+\prime}+1)]^{1/2} \\ &\times \begin{pmatrix} \ell' & 1 & \ell \\ 0 & 0 & 0 \end{pmatrix} \begin{pmatrix} \ell' & 1 & \ell \\ -m_\ell' & p & m_\ell' \end{pmatrix} \\ &\times \begin{pmatrix} N^{+\prime} & \ell & N \\ M_N - m_\ell' & m_\ell' & -M_N \end{pmatrix} \begin{pmatrix} N^{+\prime} & \ell & N \\ -\Lambda^{+\prime} & -\Lambda+\Lambda^{+\prime} & \Lambda \end{pmatrix}, \end{aligned} \tag{3.4}$$

where μ stands for the radial electronic plus nuclear part of the transition moment and the different quantum numbers have their usual meaning, the primed ones belong to the upper Rydberg states while the unprimed ones belong to the lower Rydberg states. In the case of Rydberg–Rydberg transitions in acetylene, the upper Rydberg states are not in pure decoupled case (d) as said above, thus a transition to a given $N^{+\prime}$ splits into two transitions towards $J^{+\prime} = N^{+\prime} + \frac{1}{2}$ and $J^{+\prime} = N^{+\prime} - \frac{1}{2}$, which are in turn related to the two spin-orbit limits $2\Pi_{3/2}$ and $2\Pi_{1/2}$, respectively. On the other hand, the intermediate 4s, $\tilde{G}\,^1\Pi_u$ and 3d, $\tilde{F}\,^1\Phi_u$ states conform to pure case (b).

Within the assumption of transitions between pure ℓ states, one would expect only to observe np series from the 4s intermediate state (as in figure 4). In such a case, equation (3.4) predicts only two allowed transitions, towards $N^{+\prime} = N = J = 14$, consisting of $J^{+\prime} = 14.5$ and $J^{+\prime} = 13.5$ components. These predictions are in good agreement with the limits determined for the observed series of figure 6*a*. Unfortunately, the near-zero quantum defect rules out an assignment of the upper state to an np series, as stated above. Therefore, ℓ mixing must be invoked either in the upper Rydberg states or in the intermediate Rydberg states, or in both. As far as the upper Rydberg states are concerned, zero-field p–f mixing is expected to be very small as suggested by a comparison with the p–f mixing found in the isoelectronic N_2 molecule (Huber *et al.* 1994). In addition, p–f mixing by the quadratic Zeeman effect

is also negligible in the observed energy range, as shown in figure 8 and equation (3.3). Furthermore, if p–f mixing by quadratic Zeeman effect was measurable, one would expect an increasing mixing with principal quantum number n (increasing roughly as n), which should result in rather different spectra at 'low n' from the 4s and from the 3d states. Figure 6 shows no significant difference between the two spectra, even in the lowest energy region. The most probable reason for the resemblance of both spectra and for the observation of nf series is a contribution of d orbital character in the 4s, $\tilde{G}\,{}^1\Pi_u$ state. Recent *ab initio* calculations performed by Laruelle & Lievin (1997) give a contribution of 6% of 3d, ${}^1\Pi_u$ in the $\tilde{G}\,{}^1\Pi_u$ state, which explains the similarity between the two Rydberg spectra.

In the case of a 3d (case (b)) to nf (decoupled case (d)) transition, 10 allowed transitions are predicted from equation (3.4) above, with $N^{+\prime} = J-2$ to $J+2$, leading to Rydberg series converging to ${}^2\Pi_{3/2}$ ($J^+ = 12.5$ to 16.5) and ${}^2\Pi_{1/2}$ ($J^+ = 11.5$ to 15.5). Although the $N^+ - J = 0$ transitions are expected to be the most intense, the other transitions should also appear with significant intensity. More accurate intensity calculations, taking into account the spin-orbit interaction of the core will be performed in a next step. MQDT calculations could also be performed. However, no strong rotational channel mixing is expected for such a non-penetrating series, as was found for the nf series of NO (Raoult *et al.* 1991).

The observed linewidths of the Rydberg transitions are still poorly understood. They may originate from several sources as follows.

(1) A partial overlap between the different Rydberg transitions arising from the three intermediate rotational levels populated via the band head pump line. This possibility can be ruled out on the basis of the arguments given above (see also table 2) and from further spectra obtained from isolated intermediate rotational-parity levels (Fillion *et al.* 1997) which exhibit similar line broadening.

(2) A fringe effect, as was observed in the high ns–nd series of NO by Fredin *et al.* (1987). Such a fringe effect can locally appear when two Rydberg series, converging to two different rotational limits, almost overlap for several consecutive n values and when the two related series dominate the intensity pattern of the spectrum in the corresponding spectral region, with comparison to all other allowed series. No evidence for weaker overlapping np or nf series could be found in the present spectra.

(3) The linear Zeeman effect, which should actually induce an apparent constant broadening of the $\ell = 3$ (nf) states of about $2\,\mathrm{cm}^{-1}$. For low n, a broadening of this order of magnitude is indeed observed. But with increasing n, the spectrum becomes noisier with many overlaping peaks, but with narrower linewidths. If the linear Zeeman effect was the only source of broadening and if only nf series were to be observed, a constant linewidth should be observed over the entire spectral range of figure 6.

(4) Predissociation of the nf states. These non-penetrating states can be affected by predissociation through mixing (even a very small one) with penetrating np states which are themselves very strongly predissociated. It is tempting to explain qualitatively the increasing ionization signal with increasing n, as well as the observed decreasing linewidths as being due to competition between predissociation and ionization, as was suggested earlier in this section.

Nevertheless, the analysis of these Rydberg spectra should be first clarified in terms of complete series assignments and intensity calculations before investigating the origin of the observed linewidths.

4. Conclusion

Rotational analysis of the three-photon spectra of the lowest *ungerade* supercomplexes of acetylene have led to characterization of all the electronic members of the 3d + 4s supercomplex and to a test of the high level of accuracy of the most recent *ab initio* calculations of Laruelle & Lievin (1997). These calculations have in turn provided information about the ℓ mixing (s–d) among the members of this supercomplex, and, therefore, have partially clarified the puzzling similarity between the Rydberg–Rydberg transition spectra of the high-n *gerade* states within 200 cm^{-1} of the ionization threshold.

The high-lying *gerade* nf series of acetylene have been observed for the first time. From the rotational series limits, the ionization potential has been determined to have a slightly higher value than that found from ZEKE experiments. Only two strong series could be assigned with $N^+ - J = 0$. Such a propensity rule for high Rydberg excitation (or photoionization), with no change of the core rotational state during photon excitation has already been observed in many previous experiments. A quantitative analysis is still needed to fully understand the observed intensities. From the observed trends in peak intensities and linewidths between $n = 20$ and 35, one could invoke an increasing p–f mixing by quadratic Zeeman effect which would explain simultaneously the narrowing of the lines at high energies (since no Zeeman broadening is expected for np series) as well as the increasing complexity of the spectrum. On the other hand, the np states must predissociate very rapidly in order not to have appeared as strong features in the spectra from the 4s intermediate state. Then, even if the np states show up again in the high-energy range through p–f mixing or through an n-changing competition between predissociation and ionization, the linewidth narrowing cannot be qualitatively understood.

Another plausible relaxation mechanism for these high-lying Rydberg states is isomerization into the vinylidene radical. This process might compete very efficiently with predissociation into C_2H+H, or C_2+H_2, or CH+CH fragments, through singlet–triplet mixing which is increasingly strong in this high-energy region (note that such a mixing originates from the spin-orbit coupling inside the $^2\Pi$ core, which is constant, while the singlet–triplet energy spacing decreases as n^3). The understanding of such isomerization is very important in astrophysics since vinylidene radical is supposed to be the primary precursor for large polycyclic aromatic hydrocarbons in circumstellar envelopes (Frenklach & Feigelson 1989).

An interesting alternative for studying the predissociative *ungerade* and *gerade* Rydberg states of acetylene, is to perform photofragment action spectroscopy as was demonstrated by the H-fragment action spectra of Löffer *et al.* (1996). Fragments can also be observed by further ionization and mass analysis. An important class of information for understanding the photofragmentation of circumstellar acetylene concerns the branching ratios towards different products, mainly C_2H and C_2, as a function of the excitation wavelength, between 10 and 13.6 eV. Experiments to measure these branching ratios are in progress.

We thank Dr J. Lievin and F. Laruelle for stimulating discussions and providing their theoretical results before publication. This work was supported by the CNRS through a Programme National 'Physique et Chimie du Milieu Interstellaire' contract and through a Franco-Greek PICS (no. 152) programme.

References

Ashfold, M. N. R., Dixon, R. N., Price, J. D. & Tutcher, B. 1985 *Mol. Phys.* **56**, 1185–1199.

Ashfold, M. N. R., Heryet, C. D., Prince, J. D. & Tutcher, B. 1986 *Chem. Phys. Lett.* **131**, 291–297.

Ashfold, M. N. R., Tutcher, B., Yahg, B., Jin, Z. K. & Anderson, S. L. 1987 *J. Chem. Phys.* **87**, 5105–5115.

Balko, B. A., Zhang, J. & Lee, Y. T. 1991 *J. Chem. Phys.* **94**, 7958–7966.

Beiging, J. H. & Nguyen-Q-Rieu 1988 *Ap. J.* **329**, L107–L111.

Cha, Ch., Weinkauf, R. & Boesl, U. 1995 *J. Chem. Phys.* **103**, 5224–5235.

Colin, R., Herman, M. & Kopp, I. 1977 *Proc. 21st Liège Int. Astro-physical Symp.*, pp. 355–384.

Colin, R., Herman, M. & Kopp, I. 1979 *Mol. Phys.* **37**, 1397–1412.

Dance, D. F. & Walker, I. C. 1973 *Chem. Phys. Lett.* **18**, 601–603.

Demoulin, D. 1975 *Chem. Phys.* **11**, 329–341

Demoulin, D. & Jungen, M. 1974 *Theor. Chim. Acta* **34**, 1–17.

Fahr, A. & Laufer, A. H. 1986 *J. Photochem.* **34**, 261–266.

Fillion, J. H. 1995 Thèse, Université d'Orsay.

Fillion, J. H., Shafizadeh, N. & Gauyacq, D. 1997. (In the press.)

Fillion, J. H., Campos, A., Pedersen, J., Shafizadeh, N. & Gauyacq, D. 1996 *J. Chem. Phys.* **105**, 22–30.

Fredin, S., Gauyacq, D., Horani, M., Jungen, Ch., Lefevre, G. & Masnou-Seews, F. 1987 *Mol. Phys.* **60**, 825–866.

Frenklach, M. & Feigelson, E. D. 1989 *Ap. J.* **341**, 372–384.

Gedanken, A., Raz, B. & Jortner, J. 1973 *J. Chem. Phys.* **58**, 1178–1194.

Guizard, S., Shafizadeh, N., Horani, M. & Gauyacq, D. 1991 *J. Chem. Phys.* **94**, 7046–7060.

Herman, M. & Colin, R. 1981 *J. Mol. Spectrosc.* **85**, 449–461.

Herman, M. & Colin, R. 1982 *Physica Scripta* **25**, 275–290.

Huber, K. P., Jungen, Ch., Yoshino, K., Ito, K. & Strak, G. 1994 *J. Chem. Phys.* **100**, 7957–7972.

Huggins & P. J. & Glassgold, A. E. 1982 *Ap. J.* **252**, 201–207.

Huggins, P. J., Glassgold, A. E. & Morris, M. 1984 *Ap. J.* **279**, 284–290.

Jagod, M. F., Rösslein, M., Gabrys, C. M., Rehfuss, B. D., Scappini, F., Crofton, M. W. & Oka, T. 1992 *J. Chem. Phys.* **97**, 7111–7123.

Kammer, W. E. 1970 *Chem. Phys. Lett.* **6**, 529–532

Kleppner, D., Littman, M. G. & Zimmerman, M. L. 1983 *Rydberg states of atoms and molecules* (ed. R. F. Stebbings & F. F. Dunning), pp. 73–116. Cambridge University Press.

Lafont, S., Lucas, R. & Omont, A. 1982 *Astron. Astrophys.* **106**, 201–213.

Laruelle, F. & Lievin, J. 1997. (In the press.)

Lievin, J. 1992 *J. Mol. Spectrosc.* **156**, 123–146.

Löffer, P., Lacombe, D., Ross, A., Wrede, E., Schnieder, L. & Welge, K. H. 1996 *Chem. Phys. Lett.* **252**, 304–310.

Lundberg, J. K., Yongqin Chen, Pique, J. P. & Field, R. W. 1992 *J. Mol. Spectrosc.* **156**, 104–122.

Nakayama, T. & Watanabe, K. 1964 *J. Chem. Phys.* **40**, 558–561.

Okabe, H. 1981 *J. Chem. Phys.* **75**, 2772–2778.

Okabe, H. 1983 *J. Chem. Phys.* **78**, 1312–1317.

Omont, A. 1993 *J. Chem. Soc. Faraday Trans.* **89**, 2137–2145.

Orlando, T. M., Li, L., Anderson, S. L. & White, M. G. 1986 *Chem. Phys. Lett.* **129**, 31–35.

Orlando, T. M., Anderson, S. L., Appling, J. R. & White, M. G. 1987 *J. Chem. Phys.* **87**, 852–860.

Peric, M., Buenker, R. J. & Peyerimhoff, S. D. 1984 *Mol. Phys.* **53**, 1177–1193.

Pratt, S. T., Dehmer, P. M. & Dehmer, J. L. 1993 *J. Chem. Phys.* **99**, 6233–6244.

Raoult, M., Guizard, S. & Gauyacq, D. 1991 *J. Chem. Phys.* **95**, 8853–8865.

Ridgway, S. T., Hall, D. N. B., Kleinmann, S. G., Weinberger, D. A. & Wojslaw, R. S. 1976 *Nature* **264**, 345–346.

Suto, M. & Lee, L. C. 1984 *J. Chem. Phys.* **80**, 4824–4831.

Takahashi, M., Fujii, M. & Ito, M. 1992 *J. Chem. Phys.* **96**, 6486–6494.

Truong-Bach, Nguyen-Q-Rieu, Omont, A., Olofsson, H. & Johansson, L. E. B. 1987 *Astron. Astrophys.* **176**, 285–293.

Wilkinson, P. G. 1958 *J. Mol. Spectrosc.* **2**, 387–404.

Wu, C. Y. R., Chien, T. S., Liu, G. S. & Judge, D. L. 1989 *J. Chem. Phys.* **91**, 272–280.

Discussion

R. W. Field (*Department of Chemistry, MIT, USA*). Dr Gauyacq mentioned that there is evidence that linear Rydberg states, especially triplet states, are able to isomerize to the vinylidene structure. I would like to know more about this interesting possibility.

D. Gauyacq. Photolysis experiments of acetylene performed at fixed wavelengths (193, 184.9 and 147 nm) (Satyapal & Bersohn 1991 and references therein) have shown that, in the region of the excited $\tilde{A}$ and $\tilde{B}$ valence states, photodissociation into C_2H or C_2 is not the primary process. The formation of electronically excited ($^3B_2$) triplet vinylidene radicals is shown to be a major process in this excitation energy region (Fahr & Laufer 1986). One can expect a similar situation in the excitation energy region of the Rydberg states, with a total quantum yield for dissociation significantly less than unity, and with a dominant production of a vinylidene radical. $H_2C=C$ in its lowest energy state is a singlet, which is very short lived, while the triplet excited state ($^3B_2$) is long lived and, therefore, is important in the photochemistry of this molecule. Singlet–triplet interactions in high Rydberg states should then favour isomerization into an excited triplet vivylidene.

R. W. Field. On the subject of triplet Rydberg states, I would like to report the results of a recent experiment, done in Alec Wodtke's laboratory at the University of California Santa Barbara, where perturbed gateway levels in the C_2H_2 $\tilde{A}\,^1A_u$ $3\nu_3$ state have been identified which are suitable for perturbation-facilitated double resonance studies of triplet gerade Rydberg states. Although numerous triplet perturbations of the C_2H_2 state have been known from Zeeman anticrossing (Dupre *et al.* 1991; Ochi & Tsuchiya 1991) and high-resolution UV LIF (Drabbels *et al.* 1994) experiments, these perturbers seemed to be inappropriate as gateway levels for double resonance studies of triplet Rydberg states because of their highly excited vibrational character. Highly excited vibrational levels of the *cis*- of *trans*-bent T_1 state would be useless for studies of linear triplet Rydberg states because the Franck–Condon factors for all vibrational transitions would be very small and totally unselective. It turns out that all of the triplet perturbers of C_2H_2 $\tilde{A}$ $3\nu_3$, although of dominant T_1 or T_2 or S_0 highly vibrationally excited character, contain a small admixture of one T_3 vibrational state which has significant amplitude near the linear geometry of Rydberg states (Sherrill *et al.* 1996; Vacek *et al.* 1996; Cui *et al.* 1997). Each perturbation-facilitated triplet eigenstate has *ca.* 1% character of this unique T_3 vibrational state, from which low vibrational levels of triplet Rydberg states should be Franck–Condon accessible.

I will not attempt here to describe the spectroscopic evidence for the above T_3

'assignment', but I will describe the experiment briefly. A pulsed supersonic jet of acetylene in He was excited, after the skimmer, in the 210 nm region of the $\tilde{A}$–$\tilde{X}$ $n\nu_3$ ($n = 2, 3, 4$) bands. The 134 μs flight time from the excitation region to the Auger detector (A_u, 5.1 eV work function) was sufficient to ensure that all eigenstates with greater than *ca.* 10% S_1 would radioactively decay before colliding with the Auger electrode. It is possible to distinguish between intact C_2H_2 and photofragmented C_2H or C_2 metastable species by time-of-flight and/or moving the Auger detector off axis. Strong, intact C_2H_2 signals were found in the region of the $3\nu_3$ band, but not coincident with UV emitting $S_1 \leftarrow S_0$ rotational lines. The lifetime of Auger active lines appears to be J, K_a-independent. A weak intact C_2H_2 Auger signal (as well as a stronger photofragment signal) was observed in the region of the $4\nu_3$ band, even though this is above the well known D_0^0 (HCC-H) (Mordaunt & Ashfold 1994). It turns out that the photochemistry of C_2H_2 is far more complicated than previously expected, owing to the possibility of efficiently exciting long-lived species, even at energies (147, 184.9 and 193 nm) above the dissociation limit (Okabe 1981, 1983; Seki *et al.* 1986).

M. N. R. Ashfold (*School of Chemistry, University of Bristol, UK*). I would like to draw attention to the observation of three-photon resonance enhanced MPI associated with both the $\tilde{G}\,{}^1\Pi_u$ and $\tilde{F}'\,{}^1\Phi_u$ states of C_2H_2. Our earliest study of this system (Ashfold *et al.* 1985), involving static 10 Torr samples of acetylene and acetylene-d_2, identified the $^1\Phi_u$ state but failed to show any resonance enhancements due to the dipole allowed $\tilde{G}\,{}^1\Pi_u$–$\tilde{X}\,{}^1\Sigma_g^+$ transition. Subsequent study, however, under the much lower pressure conditions prevailing in a molecular beam, revealed the expected $3+1$ REMPI via the $\tilde{G}\,{}^1\Pi_u$ state, served to highlight the possible destructive interference between one- and three-photon transition amplitudes in an optically thick medium and demonstrated third harmonic generation on the high-frequency side of the $\tilde{G}$–$\tilde{X}$ transition (Ashfold *et al.* 1986). The lesson is clear: three-photon resonance enhancements associated with transitions that are also one-photon electric dipole allowed should be investigated, as in the present study of Guayacq *et al.* (1997), at the lowest possible operating pressures compatible with adequate signal to noise ratios.

I would also like to add to Professor Field's comments concerning the photophysics of $\tilde{A}$ state acetylene molecules. H(Rydberg)TOF spectroscopy has established precise values for the C–H and C–D bond strengths in HCCH, HCCD and DCCD, including D_0(H–CCH)$= 46\,074 \pm 8\ \mathrm{cm}^{-1}$, and that the resulting ground state $C_2H(C_2D)$ fragments carry significant internal excitation, largely concentrated in the form of ν_2 bending motion (Mordaunt *et al.* 1994; Wilson *et al.* 1996). The excitation spectrum for forming H atoms in the photodissociation of HCCH 'switches on' some $560\ \mathrm{cm}^{-1}$ above D_0(H-CCH) (Suzuki *et al.* 1996). Though a full understanding of the discussion dynamics of $\tilde{A}$ state acetylene molecules still remains a little way off, the observations to date all appear to be consistent with a model in which those $\tilde{A}$ state acetylene molecules that predissociate do so via mixing with a neighbouring triplet excited state whose subsequent fragmentation (to ground state products) involves passage through a rather tightly constrained non-planar transition state, the saddle point for which lies some $560\ \mathrm{cm}^{-1}$ above the asymptotic energy associated with ground state fragment products.

G. Duxbury (*Department of Physics and Applied Physics, University of Glasgow, UK*). Could the observation of only high angular momentum states from the 3d + 4s supercomplex be due to the creation of an angular momentum barrier which,

for high values of the angular momentum quantum number, turns off the rapid predissociation?

D. Gauyacq. High angular momentum Rydberg states should not significantly participate to a potential energy barrier, turning off the rapid predissociation. These high-ℓ states are essentially *decoupled* from the core and, therefore, do not participate to the core rotation or to any nuclear motion which would lead to an angular momentum barrier. Nevertheless, these high-ℓ states have a very diffuse electronic wavefunction with a small amplitude in the inner region for the *electronic coordinate*, in which predissociation occurs (the so-called core region). This explains qualitatively why non-penetrating high-ℓ states are more stable with respect to predissociation. The real situation is always more complex because ℓ-mixing is very common in molecules and results into indirect predissociation through mixing with low-ℓ penetrating states.

Additional references

Cui, Q., Morokuma, K. & Stanton, J. F. 1997 *Ab initio* studies on the photodissociation of C_2H_2 from the S_1 (^1A_u) state. Non-adiabatic effects and S–T interactions. (In the press.)

Drabbels, M., Heinze, J. & Meerts, W. L. 1994 *J. Chem. Phys.* **100**, 165.

Dupre, P., Jost, R., Lombardi, M., Green, P. G. & Field, R. W. 1991 *J. Chem. Phys.* **152**, 293.

Gauyacq, D., Fillion, J.-H. & Shafizadeh, N. 1997 *J. Chem. Phys.* (Submitted.)

Hashimoto, N. & Suzuki, T. 1996 *J. Chem. Phys.* **104**, 6070–6073.

Mordaunt, D. H. & Ashfold, M. N. R. 1994 *J. Chem. Phys.* **101**, 2630–2631.

Ochi, N. & Tsuchiya, S. 1991 *Chem. Phys.* **152**, 319.

Satyapal, S. & Bersohn, R. 1991 *J. Phys. Chem.* **95**, 8004–8006.

Seki, K., Nakashima, N., Nishi, N. & Kinoshita, M. 1986 *J. Chem. Phys.* **85**, 274.

Sherrill, C. D., Vacek, G., Yamaguchi, Y. & Schaefer III, H. F. 1996 *J. Chem. Phys.* **104**, 8507.

Vacek, G., Sherrill, C. D., Yamaguchi, Y. & Scheafer III, H. F. 1996 *J. Chem. Phys.* **104**, 1774.

Wilson, S. H. S., Reed, C. L., Mordaunt, D. H., Ashfold, M. N. R. & Kawasaki, M. 1996 *Bull. Chem. Soc. Japan* **69**, 71–76.